

Trajectory Optimization for Dynamic Grasping in Space using Adhesive Grippers

Roshena MacPherson, Benjamin Hockman, Andrew Bylard,
Matthew A. Estrada, Mark R. Cutkosky, Marco Pavone *

Abstract Spacecraft equipped with gecko-inspired dry adhesive grippers can dynamically grasp objects having a wide variety of featureless surfaces. In this paper we propose an optimization-based control strategy to exploit the dynamic robustness of such grippers for the task of grasping a free-floating, spinning object. First, we extend previous work characterizing the dynamic grasping capabilities of these grippers to the case where both object and spacecraft are free-floating and comparably sized. We then formulate the acquisition problem as a two-phase optimization problem, which is amenable to real time implementation and can handle constraints on velocity, control, as well as integer timing constraints for grasping a specific target location on the surface of a spinning object. Conservative analytical bounds for the set of initial states that guarantee feasible grasping solutions are derived. Finally, we validate this control architecture on the Stanford free-flyer test bed—a 2D microgravity test bed for emulating drift dynamics of spacecraft.

1 Introduction

Recently, in an effort to alleviate some of the tasks performed by astronauts, there has been increased interest in the use of small assistive free-flying robots (AFF) for grasping and manipulating objects inside and outside spacecraft. One such example is the Smart SPHERES teleoperated test bed, which was developed to perform various intra-vehicular activities aboard the International Space Station (e.g., camera work and environmental monitoring), as well as to serve as a robotics research

* Roshena MacPherson, Benjamin Hockman, Matthew A. Estrada, and Mark R. Cutkosky are with the Department of Mechanical Engineering, Stanford University, CA 94305. Andrew Bylard and Marco Pavone are with the Department of Aeronautics and Astronautics, Stanford University, CA 94305. Emails: {roshenam, bylard, bhockman, estrada1, cutkosky, pavone}@stanford.edu. This work was supported by NASA under the Space Technology Research Grants Program, Grant NNX12AQ43G, and Early State Innovations, Grant NNX16AD19G.

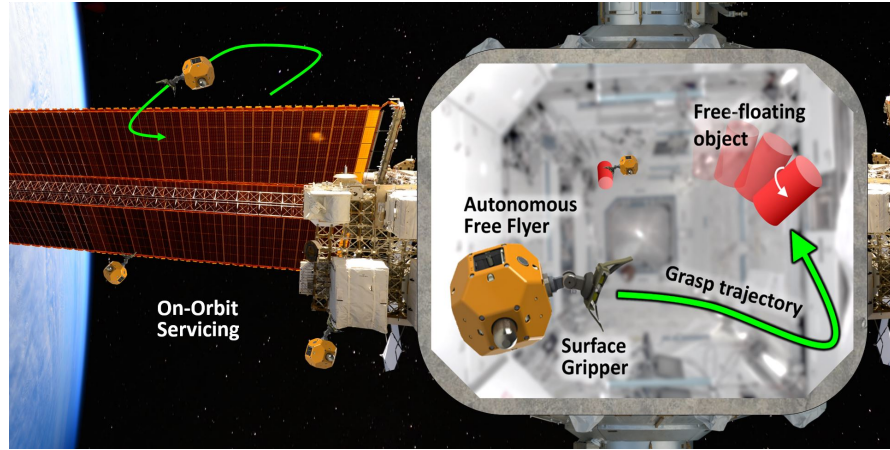


Fig. 1: Autonomous free flying spacecraft equipped with dry adhesion surface grippers may assist astronauts inside and outside the space station. This paper investigates optimal control strategies for autonomous perching and acquisition of free-floating, tumbling objects.

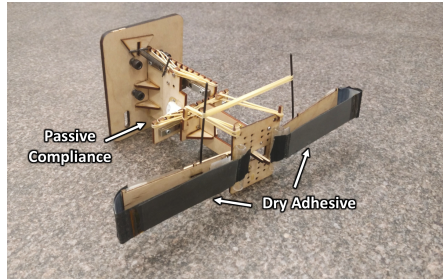
platform in microgravity [1]. Enabling AFFs to autonomously grasp and manipulate objects has the potential to make many human operations safer and more efficient by reducing time spent performing repetitive tasks and on EVAs (see Fig. 1). Autonomous object manipulation may also enable a wide range of new applications that are too dangerous, complex, or expensive for astronauts, such as the assembly of large-scale space structures or the removal of space debris [2].

Traditionally, most grasping devices, especially in space, have relied on robotic hands that either pinch opposing faces of the target (“force closure”) or grapple around its features to secure it (“caging grasp”). The precision of this operation typically requires that the target be stationary relative to the gripper for successful acquisition. For example, in [3] and [4], the authors assume that target objects have a grappling fixture for caging [3] or pinching [4] and plan the spacecraft’s trajectory such that its end effector velocity matches that of the grappling feature. However, velocity matching often imposes a heavy burden on control precision and fuel expenditure.

Grippers that utilize *dry surface adhesion* represent a promising alternative. Inspired by the adhesive properties of geckos’ feet, several grippers have been developed using gecko-like materials that can adhere to any smooth, flat or curved surface *simply by touching them* [5, 6]—thus, broadening the class of possible grasp locations from a small set of features to a larger (continuous) space of feature-*less* surfaces. Furthermore, when paired with a compliant wrist mechanism, these grippers can *dynamically* engage objects with high relative velocity—a key advantage for capturing drifting objects in space [7]. Previous work by the authors investigated the performance of one such gripper designed to grasp a translating and rotating object [6] (see Fig. 2). A passive cylindrical object, free-floating on frictionless air bearings, was thrown at a stationary gripper on Stanford’s planar microgravity test

bed (see Fig. 4). The gripper, fixed to the inertial frame, was able to catch the object over a wide range of contact velocities. By systematically probing the dynamic limitations of the gripper in simulations and experiments, an envelope of contact states amenable for reliable grasping was empirically constructed—henceforth referred to as the “grasping envelope.” In this paper, we investigate how such dynamic surface grasping can be leveraged to develop robust control laws for grasping objects in space.

Fig. 2: A curved-surface gripper utilizes gecko-inspired adhesive materials to robustly grasp a variety of objects. Two opposing fingers passively collapse onto any curved smooth surface upon contact, by triggering a bistable mechanism. The gripper is mounted on a passive compliant wrist that allows it to absorb impact energy. See [8] for details.



From a control standpoint, adhesive grippers eliminate the need to deliberately coordinate finger contact forces, allowing the precision grasping task to be simplified to a *rendezvous and docking problem*—a well-studied problem having a rich body of literature. Specifically, a variety of optimization-based approaches have been devised for the problem of spacecraft rendezvous and docking, including [9], which treats some of the constraints as soft penalties in the cost function. This allows the problem to be formulated as a Quadratic Program (QP), thus enabling real-time implementation. Similarly, [10] restricts each phase of the problem (long-range rendezvous, short-range docking, etc.) to be formulated as either a Linear Program (LP) or a QP for fast, online execution. In [11], the authors applied MPC to the rendezvous and docking of a spacecraft with a non-rotating platform in circular orbit around the Earth. They extended this work in [12] to the case of a rotating/tumbling object, imposing state constraints to avoid debris. In a similar vein, we propose an optimization-based approach to the related problem of dynamic grasping, consisting of a two-phase optimal control architecture that is amenable to the complex dynamics and terminal constraints characterizing adhesive grippers, and integer timing constraints for grasping a specific location on a spinning body.

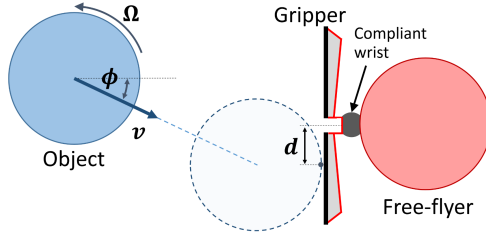
Specifically, the contribution of this paper is threefold. First, in Section 2, we extend our previous work in [6] on characterizing the grasping envelope of a curved surface gripper to the case where both spacecraft and object are free floating and in relative motion. Second, in Section 3 we formulate the problem of grasping spinning, featureless objects as a two-phase optimal control problem and derive conservative analytical bounds for the set of initial states that guarantee feasible grasping solutions. Finally, we validate the controller in simulation and through a variety of experiments on a custom free-floating spacecraft test bed (Section 4).

2 Grasping Envelope

In order to leverage the dynamic grasping capabilities of adhesive grippers for robust object acquisition, some model of the set of “graspable” contact states is required. This *grasping envelope* is a complex function of the gripper design, object shape and surface, and the highly nonlinear behavior of the dry adhesives. First order insights for defining this envelope can be derived from analytical models and simulations (as was done in [6]), but a more complete characterization relies on systematically probing the boundaries experimentally. In previous work, Estrada et al. [6] characterized the envelope of a gripper fixed to the inertial frame through a passive compliant wrist, which is akin to the case in which the target object is significantly less massive than the spacecraft. However, for small AFFs that often perch or grasp larger objects, this is often not the case. Accordingly, our first step is to extend those results to the more general case in which both object *and* spacecraft are floating and of comparable mass.

For planar motion, the contact state can be uniquely described by four parameters, namely, the offset of the contact from the center of the gripper (d), and the relative velocity, decomposed as the linear (v) and angular (Ω) speeds and angle of attack (ϕ) (see Fig. 3). Thus, the grasping envelop can be viewed as a closed set $(v, \Omega, \phi, d) \in \mathbb{R}^4$ centered at $(\mu_v, 0, 0, 0)$ and symmetric about $d = 0$.

Fig. 3: The contact state between the spinning cylindrical object and free-flyer is parameterized with four variables as show in this top-down view: relative speed (v), angular velocity (Ω), angle of attack (ϕ), and offset (d). Note that these parameters are defined with respect to the free-flyer, which may also be moving.

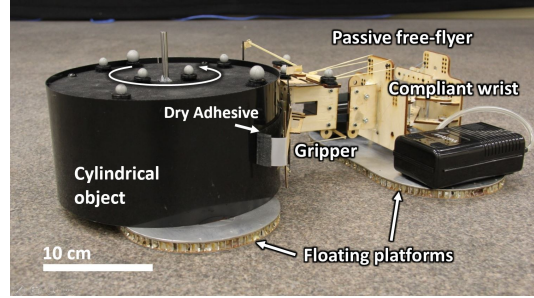


For imposing terminal velocity constraints in the grasping problem, it is most important to characterize the relationship between speed and angle of attack, which can then be translated into normal and lateral velocity constraints. In other words, by varying v and ϕ and holding d and Ω constant, one can experimentally construct a 2D slice within the 4D grasping envelope by observing successful and unsuccessful grasps.

All experiments were conducted on the Stanford free-flyer test bed—a 3x4 m granite table calibrated to be extremely flat and level—on which robotic platforms can float using frictionless air bearings, simulating a 2D microgravity environment (See Fig. 4). In nearly the exact same setup as in [6], a smooth cylindrical object (1.6 kg, 11 cm radius) was fixed to a floating platform such that it could be spun and launched towards a gripper, which was also mounted on a floating platform. An OptiTrack motion capture system was used to measure the trajectories of the object, free-flyer robot, and its attached gripper to sub-millimeter precision at 120 Hz.

About fifty trials were run, varying the object’s speed and angle of attack for each of two scenarios: (1) a high-mass free-flyer (4.2 kg or roughly 2.5 times the mass of

Fig. 4: Grasping experiment on the Stanford free-flyer test bed. A cylindrical object mounted on a frictionless air-bearing platform collides and attaches to another free floating platform equipped with a curved surface gripper. The dry adhesive fingers and compliant wrist are able to reliably secure the object over a wide range of dynamic contacts.



the object), and (2) a low-mass free-flyer (1.7 kg or roughly the same mass as the object). The results in Fig. 5 show the data for both of these scenarios compared with data for a fixed gripper from [6]. Two analytical bounds were proposed in [6] to segment the successful and unsuccessful grasps and correlate them to the two dominant failure modes, which were: (A) a minimum normal impulse that was required to depress the gripper’s passive trigger mechanism², and (B) a maximum angular impulse that the gripper’s compliant wrist could absorb after attaching. These bounds are still good predictors of failure for a floating free-flyer, however the normal and angular impulse must now also account for the movement of the free-flyer after collision. Thus, as the mass of the free-flyer is reduced, the minimum speed needed for the object to passively engage the gripper increases, the tolerable angular momentum of the object decreases, and overall, the grasping envelope shrinks.

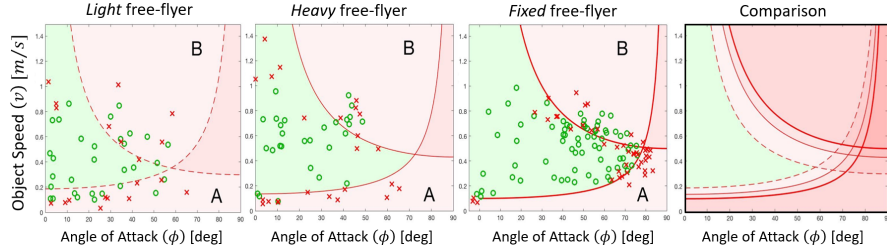


Fig. 5: Grasping envelopes relating speed (v) and angle of attack (ϕ) for a non-spinning object contacting the gripper with zero offset (d). The left three plots show data collected for a light (1.7 kg), heavy (4.2 kg), and fixed free-flyer, respectively. The green o’s and red x’s depict successful and unsuccessful trials. The right plot overlays the approximate envelope bounds for each of the three cases, indicating generally tighter bounds for lighter free-flyers.

For high-speed collisions, an additional failure mode was observed, whereby the floating free-flyer rebounds before the gripper can fully close around the object. This phenomenon involves the mechanical response of gripper’s compliant mount and the response time of the bistable closing mechanism. In [13], Yoshida discusses the contact dynamics between a robotic arm and a floating satellite and shows that appropriate *impedance matching* can mitigate this effect. Future work will consider

² Future gripper designs will incorporate an automatic trigger, eliminating the minimum normal impulse requirement.

similar methods of impedance matching using tunable wrist compliance [8] to reduce this rebound effect. For the grasping controller discussed in Sect. 3, we will simply enforce a constraint on the maximum speed.

3 Autonomous Grasping

In this section we formally state the control problem we wish to address, devise a two phase formulation for its solution using optimal control techniques, and discuss feasibility guarantees and implementation details. We highlight that our problem formulation and tests are limited to planar motion; the generalization to 3D is possible and will be addressed in future work. Furthermore, we make two key assumptions: (1) the environment is obstacle-free, and (2) orbital dynamics can be ignored. In practice, the full motion planning problem for grasping would be decoupled into an initial rendezvous phase using a kinodynamic motion planner (e.g., [14]) to negotiate obstacles over an arbitrary distance, which transitions to this final controller within a close, obstacle-free vicinity. Similarly, the short timescales for this grasping problem make higher-order effects due to orbital dynamics negligible. Sect. 3.1 states the dynamics of the problem, Sect. 3.2 discusses the decoupled control architecture and desired contact geometry, Sect. 3.3 derives the control law for phase 1, Sect. 3.4 derives the control law for phase 2, and Sect. 3.5 derives conservative analytical bounds for the region of attraction.

3.1 System Dynamics

We consider an autonomous docking between a target object (T) and a spacecraft (S) equipped with a dry adhesive gripper. The target object has a circular shape of radius r_T , mass m_T , and rotates with constant angular velocity ω_T . The spacecraft has a gripper located distance l_S from its center of mass S_{cm} , and rotates with angular velocity $\omega_S(t)$. We define a point T_g on the surface of T that represents the target point for contact (e.g., a part of the target surface that is particularly suitable for grasping). Right-handed orthogonal bases, n , t , and s are fixed in the inertial frame, target object, and spacecraft, respectively, rotated by angles θ_S and θ_T . The position vector from T_{cm} to S_{cm} can be written as $\mathbf{r}_S = x\hat{n}_x + y\hat{n}_y$ and its derivative, $\mathbf{v}_S = \dot{x}\hat{n}_x + \dot{y}\hat{n}_y$. This notation is summarized in Fig. 6. The double-integrator dynamics of the spacecraft are simply,

$$\ddot{x} = u_x, \quad \ddot{y} = u_y, \quad \ddot{\theta}_S = u_{\theta_S}, \quad (1)$$

where u_x and u_y represent the translational control inputs (actuated, e.g., via thrusters), and u_{θ_S} represents the independent angular control input (actuated, e.g., via a reaction wheel). For convenience, we can rewrite the dynamics with respect to a new basis, e , as

$$\dot{v}_r - \frac{v_\theta^2}{r} = u_r, \quad \dot{v}_\theta + \frac{v_r v_\theta}{r} = u_\theta, \quad (2)$$

where $\mathbf{r}_S = r\hat{e}_r$, and $\mathbf{v}_S = v_\theta\hat{e}_\theta + v_r\hat{e}_r$. This form will be useful for deriving the alignment controller in Sect. 3.3. Note that thruster arrangements on spacecraft typ-

ically yield nonuniform maximum thrust capabilities *in the body frame*. Thus, most generally, $u_{r,\max}$ and $u_{\theta,\max}$ are functions of θ_S . However, for simplicity, we will impose a conservative inner approximation on the control constraints:

$$u_r^2 + u_\theta^2 \leq u_{\max}^2, \quad u_{\max} = \min[u_{\max}(\theta_S)], \quad (3)$$

which allows the exact mapping to thruster firings to be abstracted as a lower level controller.

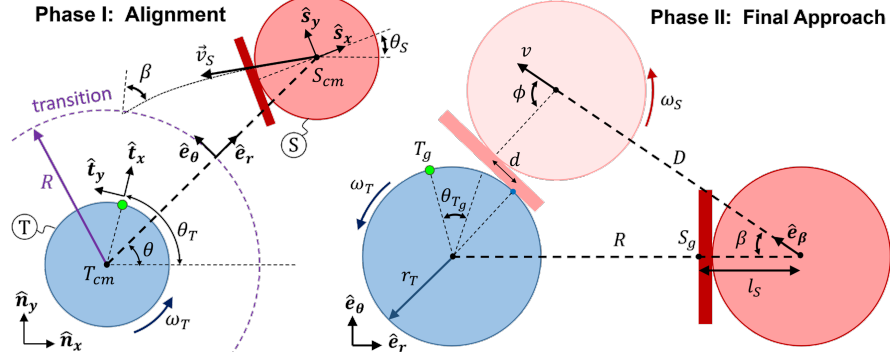


Fig. 6: Geometry of the grasping problem. The initial alignment phase (left) steers the spacecraft towards some desired approach trajectory, defined by β , at which point the final approach phase (right) tracks a straight-line to ensure proper timing and contact geometry.

3.2 Control Architecture

The grasping problem is constrained in three fundamental ways: (1) constraints on the control input, (2) a constraint on the contact location on the surface of the rotating target, and (3) dynamic contact constraints imposed by the gripper, as characterized in [6] and Sect. 2. For a spinning object, the constraint on the contact location imposes a coupled relationship on the pose and timing of contact, according to $t_f = \frac{\theta_{T_g} + 2\pi n}{\omega_T}$, where n is an integer number of rotations before collision, and θ_{T_g} encodes the contact pose. This integer constraint on the final time, combined with the complex 4D grasping envelope, makes this problem challenging to solve end-to-end as a single optimal control problem. We note that for $\omega_T \rightarrow 0$, we have $t_f \rightarrow \infty$, which leads to prohibitively slow solutions. Indeed this control approach is tailored for the case in which the target's angular velocity is faster than a simpler linear controller can handle (e.g. by “chasing” the target point). In other words, our control approach should be considered complimentary to a controller that can handle static or quasi-static cases.

Accordingly, we decompose the grasping problem into two phases. Phase 1 aligns the spacecraft’s velocity vector with the desired approach vector (Fig. 6, left) and phase 2 simply tracks this straight line trajectory and ensures proper contact timing (Fig. 6, right). Importantly, the phase switch is assumed to occur sufficiently

far from the target as to guarantee a feasible, time-optimal solution—thus imposing constraints on initial conditions, as discussed in Sect. 3.5.

To define this switching condition, we must work backwards from the desired contact state within the grasping envelope. In principle, an appropriate selection of approach trajectory can map to *any* desired point in the grasping envelope. Practically, however, the spacecraft cannot spin arbitrarily fast to match the object. In fact, it is often desired for the spacecraft to have *zero* angular velocity for robust trajectory tracking (i.e. so that thrusters are not spinning). Therefore, by forcing $\omega_S = 0$, the relative angular velocity at contact is simply that of the target object, ω_T .

There are many ways in which the remaining contact states (v^*, ϕ^*, d^*) may be chosen. Given some estimate of the grasping envelope, one strategy would be to inscribe a maximum radius sphere within the (3D) slice defined by $\Omega = \omega_T$. The center of this sphere is one measure of the most robust target point. Therefore, given some appropriate selection of contact state $(v^*, \omega_T, \phi^*, d^*)$, the geometry of the approach trajectory in phase 2 (see Fig. 6, right) can be uniquely defined as:

$$v = v^*, \quad \phi = \phi^*, \quad \omega_S = 0, \quad \beta = \sin^{-1} \left(\frac{d^* \cos \phi^* + (l_S + r_T) \sin \phi^*}{R} \right), \quad (4)$$

where R is the distance of the spacecraft at the beginning of phase 2. Interestingly, as discussed in [6], this optimal target point often corresponds to a non-zero offset and angle of attack for spinning objects—a key difference from traditional grippers.

Note that this paper does not address attitude control, which is a function of the specific arrangement of actuators for a given spacecraft. For the planar motion with a reaction wheel considered here, the (1D) solution is trivial. We simply assume that the spacecraft is able to rotate to the desired heading for grasping within t_f .

3.3 Phase 1: Alignment

The goal of the initial alignment phase is to drive the spacecraft to the desired approach vector computed by (4) in minimum time. Specifically, the final switching condition is met at t_s when,

$$\frac{v_\theta(t_s)}{-v_r(t_s)} = \tan \beta. \quad (5)$$

Intuitively, this can be thought of as applying some control input to effectively “rotate” the velocity vector until it points at the desired contact location. Note from Eq. (4) that β is a function of R , which is time-varying. Thus, while β cannot be computed exactly *a priori*, Eq. (5) can easily be evaluated at each time step to check for the switching condition.

The control input to achieve this in *minimum time* is simply a maximum thrust *normal* to the approach vector, specifically:

$$u_\theta^*(t) = u_{\max} \cos \beta \frac{-v_\theta(t)}{|v_\theta(t)|}, \quad u_r^*(t) = u_{\max} \sin \beta \frac{v_r(t)}{|v_r(t)|}. \quad (6)$$

Since β is often small (within 10° for typical parameters and zero in the nominal case), the dominant component of thrust is normal to the the spacecraft's position vector (\mathbf{r}_S), effectively arresting the spacecraft's angular momentum about the target. Furthermore, the geometry of this thrust is such that the spacecraft's speed will always decelerate. Thus, a total speed constraint (that is not initially violated) will remain obeyed. An apparent drawback of this approach is the inability to directly consider position constraints, which may arise due to, e.g., narrow corridors within the ISS. However, as a last stage in a higher level planning framework, this controller can make some assumptions about the allowable set of initial states (e.g. from a kinodynamic planner) that guarantee a collision-free "approach corridor."

3.4 Phase 2: Final Approach

After aligning the velocity vector (along \hat{e}_β) in phase 1, the goal for phase 2 (starting at t_0) is to track this straight-line trajectory to intercept the target object at state (v^*, ϕ^*) and location T_g using *minimum fuel*. Indeed, a periodic constraint is imposed on the final time:

$$t_f = \begin{cases} \frac{\theta_{T_g}(t_0) + 2\pi n}{\omega_T}, & \omega_T < 0 \\ \frac{2\pi(1+n) - \theta_{T_g}(t_0)}{\omega_T}, & \omega_T > 0 \end{cases}, \quad \theta_{T_g}(t_0) = \theta_T(t_0) - \theta(t_0) - \phi^* + \beta + \frac{d^*}{r_T}, \quad (7)$$

where n is the integer number of full revolutions of the target object before contact. The minimum feasible n also corresponds to the *minimum time* solution. For some choice of n , we can formally state the 1D input-constrained minimum fuel optimal control problem:

$$\begin{aligned} \min \quad & \int_0^{t_f} |u(t)| dt \\ \text{s.t.} \quad & \dot{X} = AX + Bu \\ & X(0) = [r, v_0]^T \\ & X(t_f) = [D, v_f]^T \\ & u_{\min} \leq u(t) \leq u_{\max} \end{aligned} \quad (8)$$

where $X = [r, v]$, $\dot{r} = v$, $D = \frac{1}{\cos\beta} [R - r_T \cos(\phi - \beta) - l_S \cos(\beta - \phi) - d \sin(\beta - \phi)]$, and A and B represent the dynamics of a 1D double integrator. It is known that the solution to an input constrained minimum-fuel optimal control problem (where the system is controllable) will have a bang-off-bang form [15]. Additionally, for our specific problem, there are a family of fuel-optimal solutions corresponding to the choice of n . For an initial radius (D) sufficiently large, an optimal solution is to fire the thrusters one time in an off-bang-off regime, whereby the timing and duration of the firing determines the impact speed (v_f) and time (t_f). The total time is given by the sum of the initial coast phase (τ_1), acceleration phase (τ_2), and final coast phase (τ_3). Similarly, the total distance traveled (D) can be decomposed into three phases. With appropriate manipulation, this allows the timing to be computed as:

$$\tau_1 = \frac{D + v_f(\tau_2 - t_f) - \frac{|v_f^2 - v_0^2|}{2u_{\max}}}{|v_f - v_0|}, \quad \tau_2 = \frac{|v_f - v_0|}{u_{\max}}. \quad (9)$$

Note that this solution is only valid for $0 \leq \tau_1 \leq t_f - \tau_2$ and $\tau_2 < t_f$. In other words, a single-fire solution may not exist for spacecraft that starts too far away, approaches too fast, too slow, or when $v_0 \approx v_f$. For this case when $\tau_1 \geq t_f - \tau_2$, a two-fire, bang-off-bang control is optimal, whereby the spacecraft immediately thrusts for duration τ_1^* , coasts for τ_2^* at speed v_2 , and thrusts for the remaining τ_3^* . Similar to (9), the timing of the firing can be computed as:

$$\tau_1^* = \frac{|v_2 - v_0|}{u_{\max}}, \quad \tau_3^* = \frac{|v_f - v_2|}{u_{\max}}, \quad v_2 = \frac{Du_{\max} - \frac{1}{2}|v_2^2 - v_0^2| - \frac{1}{2}|v_f^2 - v_2^2|}{u_{\max}t_f - |v_2 - v_0| - |v_f - v_2|}. \quad (10)$$

This solution is also only valid for $\tau_1^* + \tau_3^* \leq t_f$. Otherwise, the timing mismatch at t_0 is too large for a bang-off-bang regime to compensate. However, an appropriate constraint on the initial state (discussed in Sect. 3.5), can guarantee that *either* a single-fire solution (Eq. (9)) or two-fire solution (Eq. (10)) exists.

3.5 Approximate Region of Attraction

In summary, given some initial state, the two-phase control proceeds as follows:

1. Select a desired location on the surface of the target to grasp, T_g .
2. Using some model for the grasping envelope, select a robust target point $(v^*, \omega_T, \phi^*, d^*)$ as the desired contact state.
3. Execute the control for phase 1 according to (6).
4. Watch for terminal condition given by (5) and switch to phase 2 when triggered.
5. Compute optimal single-fire control inputs according to (9).
6. If infeasible, compute the two-fire optimal control solution according to (10).
7. Execute phase 2 controller, optionally with a closed-loop tracking controller (e.g., LQR), to drive the spacecraft to the desired contact state.

In order to stitch this controller to a preceding planner, we would like to formally characterize the set of initial states from which a feasible solution is guaranteed—corresponding to, for example, the goal region of a kinodynamic planner. First, Eqs. (9) and (10) will be used to derive a minimum distance, D_{\min} at which phase 2 must begin to guarantee a feasible solution for *any possible target point*. Then, a conservative linearization of the dynamics given by Eqs. (2) and (6) will provide an inner approximation of the backwards reachable set to achieve this transition.

3.5.1 Region of Attraction for Phase 2

To derive the minimum distance D_{\min} for phase 2, we start by realizing that in order to guarantee feasibility for *any* choice of T_g (i.e. at least one feasible choice of n), then it is sufficient to guarantee that a solution exists for all $t_{f,\min} \leq t_f \leq t_{f,\min} + 2\pi/\omega_T$ (i.e., the time the target takes to complete one full rotation).

For the single-fire solution given by eq. (9), the minimum distance D_{\min} can be derived by setting the difference in timing between the slowest solution and fastest solution exactly equal to one rotation period: $t_{f,\max} - t_{f,\min} = \frac{2\pi}{\omega_T}$. For example, in the case when the spacecraft needs to slow down (i.e. $v_f < v_0$), the slowest solution is to apply u_{\max} immediately and coast at v_f until impact, and the fastest solution is to wait until just before impact to apply u_{\max} . Substituting this into (9) and (10) and solving for D_{\min} , we have

$$D_{\min} = \frac{2\pi v_0 v_f}{\omega_T |v_f - v_0|} + \frac{|v_f^2 - v_0^2|}{2u_{\max}}. \quad (11)$$

The second term corresponds to the distance traveled during thrusting, and the first term represents the distance required to adjust phasing by up to 2π .

For a two-fire solution, we can take the same approach by computing $t_{f,\max} - t_{f,\min} = \frac{2\pi}{\omega_T}$. In this regime, $t_{f,\min}$ is achieved by accelerating as long as possible before immediately decelerating to hit T at v_f (i.e. $\tau_2^* = 0$), and $t_{f,\max}$ is the exact opposite. However, in some cases $t_{f,\max} = \infty$, corresponding to the case when the spacecraft can fully stop before accelerating. Thus eq. (10) can be manipulated in a similar way to solve for D_{\min}^* , the minimum distance required for a guaranteed solution in a two-fire regime:

$$D_{\min}^* = \min \left\{ \frac{v_0^2 + v_f^2}{2u_{\max}}, \left| \frac{\pi}{2\omega_T} - \frac{v_0 + v_f}{2u_{\max}} \right| \sqrt{(v_0 - v_f)^2 + \frac{2\pi u_{\max} (v_0 + v_f)}{\omega_T} - \frac{\pi^2 u_{\max}^2}{\omega_T^2}} \right\}. \quad (12)$$

3.5.2 Region of Attraction for Phase 1

Now that we have characterized the minimum distance required at the phase 2 transition, we would like to compute the backwards reachable set through the control input during phase 1 to find a set of initial states for which a solution is guaranteed. However, the coupled, second order nonlinear dynamics from Eqs. (2) and (6) cannot be solved in closed form. Instead, we can solve for a conservative approximation of the minimum time, $\hat{t}_s \geq t_s$ by linearizing the dynamics:

$$\dot{v}_r = u_r + \frac{v_\theta^2}{r} \approx 0, \quad (13)$$

$$\dot{v}_\theta = u_\theta - \frac{v_r v_\theta}{r} \approx u_{\theta,\text{eff}} = \frac{u_\theta - v_r(0)v_\theta(0)}{r(0)}, \quad (14)$$

where $u_{\theta,\text{eff}}$ represents the reduced effective control in the \hat{e}_θ direction. For $v_r(0) < 0$ (i.e. moving towards the target), u_θ and $C(t) = v_r(t)v_\theta(t)/r(t)$ always have the same sign. Furthermore, it can be shown that $\text{sgn}(\frac{dC}{dt}) = -\text{sgn}(C(t)) \quad \forall t \in (0, t_s)$, if $(v_\theta^2 + 2|v_r v_\theta|)/r \leq u_{\max}$. In other words, the magnitude of C is monotonically decreasing, and $|\dot{v}_\theta| \geq |u_{\theta,\text{eff}}| \quad \forall t \in (0, t_s)$. Thus, $\dot{v}_\theta \approx u_{\theta,\text{eff}}$ will serve as a conservative approximation for computing \hat{t}_s .

Similarly, since it is assumed that $v_r < 0$, the approximation that $\dot{v}_r \approx 0$ yields a conservative approximation of the inward radial distance traveled (Δr_{\min}) if $\dot{v}_r \geq 0$,

which is true for $\beta \leq \sin^{-1}(v_\theta^2/(ru_{\max}))$. Finally, we can use the linearized dynamics given by (13) and (14) to compute \hat{t}_s and Δr_{\min} :

$$\hat{t}_s = \frac{v_\theta(0) + v_r(0) \tan \beta}{u_{\theta,\text{eff}}}, \quad \Delta r_{\min} = v_r(0) \hat{t}_s. \quad (15)$$

Combining Eqs. (11), (12), and (15), we can express the total initial distance the spacecraft must be from the target as:

$$r \geq \min(D_{\min}, D_{\min}^*) + \Delta r_{\min}. \quad (16)$$

Note that the initial velocity in phase 2 (v_0 in Eqs. (11) and (12)) is now approximated by $|v_r(0)|$. In summary, the set of initial states for persistent feasibility is defined by (16) and the following assumptions:

$$v_r < 0, \quad \frac{v_\theta^2 + 2|v_r v_\theta|}{r} \leq u_{\max}, \quad \beta \leq \sin^{-1} \left(\frac{v_\theta^2}{ru_{\max}} \right). \quad (17)$$

While these are complicated, interdependent expressions, in the context of a sampling-based motion planner, they are cheap to evaluate (i.e. query the goal state).

4 Experimental Results

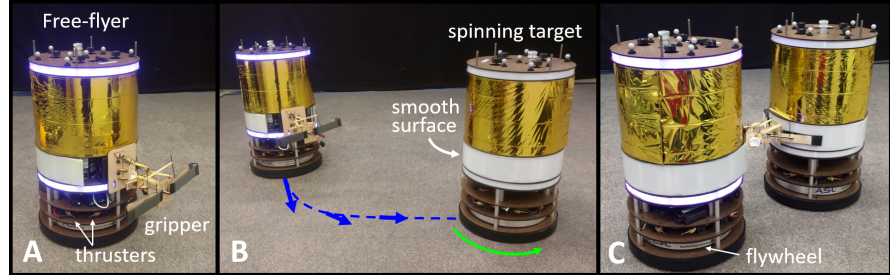


Fig. 7: Autonomous grasping experiments on the Stanford free-flyer test bed. (A) A free-flying robot floats on frictionless air bearings and is equipped with eight compressed gas thrusters and a flywheel. (B) The trajectory controller developed in Sect. 3 is executed on-board to dynamically grasp (C) a translating and spinning target.

The two-phase grasping controller developed in Sec 3 was implemented on the Stanford free-flyer test bed (see Fig. 7). A simple PD controller was used to control free-flyer attitude in Phase 2. A passive target object was manually spun and pushed at some initial coasting velocity. The free-flying robot equipped with eight thrusters and a reaction wheel was pushed at varying initial velocities (within the region of attraction), immediately executing the grasping controller. Figure 8 displays five (of 16) example trajectories overlaid on the (ideal) simulated trajectory. A video of one example trajectory can be found at: <https://www.youtube.com/playlist?list=PL8-2mtI1FIJrHMGNeKmHnkB1XBD0iKvto>.

Overall, there is good agreement between the measured and simulated trajectories. Most of the deviation can be attributed to modeling errors—in particular, the changing mass of the free-flyers as the CO₂ tanks drain (to be addressed with online system identification in future work). We also observed some timing errors during the second approach phase which caused the free-flyer to occasionally miss the target point. This is because the reference trajectory for the second phase was computed immediately after phase one, which can result in mis-timed grasps when unanticipated modeling errors such as table friction are present. Future experiments will incorporate an MPC-style implementation of the phase two controller that constantly recomputes the reference trajectory for more robust grasping.

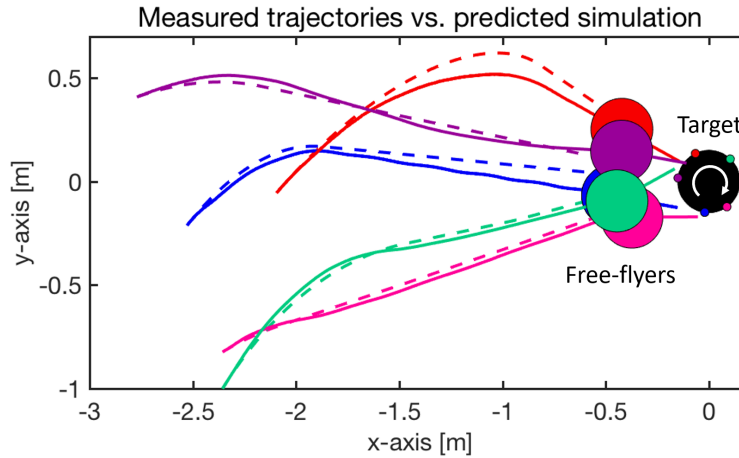


Fig. 8: Measured motion capture data for three example trajectories (solid lines) of a free-flying robot grasping a spinning target (black) overlaid with simulated predictions (dashed lines). The points on the surface of the target represent the locations of the target point (T_g) upon impact for the corresponding color. Gripper orientation is indicated by a straight line.

5 Conclusions

In this paper we presented an optimal control approach for the problem of dynamic grasping of tumbling objects in space using gecko-inspired adhesive grippers. We extended the characterized grasping envelope for a curved surface gripper to the case when both the spacecraft and target object are free floating and of comparable mass. We developed a two-phase control architecture that decomposes the grasping problem into an initial alignment phase and final approach phase, each of which with time optimal solutions. A conservative inner approximation of the region of attraction for initial states was derived analytically to serve as a terminal goal region for a preceding motion planner. Experimentation is ongoing, but the preliminary results constitute one of the first successful demonstrations of autonomous surface grasping in a high-fidelity spacecraft analog test bed.

This paper leaves numerous important extensions open for future research. First, it is important to extend the controller to handle non-cylindrical objects, whereby

surface target selection should be addressed in a more principled way. Second, we plan to introduce an actuated arm that allows for more robust acquisition through active damping and impedance matching, and also for manipulation tasks. Third, we plan to extend this controller and gripper design to allow for out-of-plane motion. Finally, future experiments will be integrated with a preceding kinodynamic motion planner to negotiate obstacle-rich environments.

References

1. T. Fong, M. Micire, T. Morse, E. Park, C. Provencher, V. To, D. W. Wheeler, D. Mittman, J. Torres, and E. Smith. Smart SPHERES: a telerobotic free-flyer for intravehicular activities in space. In *AIAA SPACE Conferences & Exposition*, 2013.
2. R. Ambrose, I. A. D. Nesnas, F. Chandler, B. D. Allen, T. Fong, L. Matthies, and R. Mueller. 2015 NASA technology roadmaps: TA 4: Robotics and autonomous systems. Technical report, NASA, 2015.
3. F. Aghili. A prediction and motion-planning scheme for visually guided robotic capturing of free-floating tumbling objects with uncertain dynamics. *IEEE Transactions on Robotics*, 28(3):634–649, 2012.
4. P. Motaghedi. On-orbit performance of the orbital express capture system. *Proc. of SPIE*, 6958(0E), 2008.
5. H. Jiang, E. W. Hawkes, V. Arutyunov, J. Tims, C. Fuller, J. P. King, C. Seubert, H. L. Chang, A. Parness, and M. R. Cutkosky. Scaling controllable adhesives to grapple floating objects in space. In *Proc. IEEE Conf. on Robotics and Automation*, 2015.
6. M. A. Estrada, B. Hockman, A. Bylard, E. W. Hawkes, M. R. Cutkosky, and M. Pavone. Free-flyer acquisition of spinning objects with gecko-inspired adhesives. In *Proc. IEEE Conf. on Robotics and Automation*, 2016.
7. E. W. Hawkes, D. L. Christensen, E. V. Eason, M. A. Estrada, M. Heverly, E. Hilgemann, H. Jiang, M. T. Pope, A. Parness, and M. R. Cutkosky. Dynamic surface grasping with directional adhesion. In *IEEE/RSJ Int. Conf. on Intelligent Robots & Systems*, 2013.
8. M. A. Estrada, H. Jiang, B. Noll, E. W. Hawkes, M. Pavone, and M. R. Cutkosky. Force and moment constraints of a curved surface gripper and wrist for assistive free flyers. In *Proc. IEEE Conf. on Robotics and Automation*, 2017.
9. A. Weiss, M. Baldwin, R. S. Erwin, and I. Kolmanovsky. Model predictive control for spacecraft rendezvous and docking: Strategies for handling constraints and case studies. *IEEE Transactions on Control Systems Technology*, 23(4):1638–1647, 2015.
10. E. Hartley, P. A. Trodden, A. G. Richards, and J. M. Maciejowski. Model predictive control system design and implementation for spacecraft rendezvous. *Control Engineering Practice*, 20(7):695–713, 2012.
11. H. Park, S. Di Cairano, and I. Kolmanovsky. Model predictive control of spacecraft docking with a non-rotating platform. *IFAC World Congress*, 44(1):8485–8490, 2011.
12. S. Di Cairano, H. Park, and I. Kolmanovsky. Model predictive control approach for guidance of spacecraft rendezvous and proximity maneuvering. *Int. Journal of Robust and Nonlinear Control*, 22(12):1398–1427, 2012.
13. K. Yoshida, H. Nakanishi, H. Ueno, N. Inaba, and M. Oda. Dynamics, control and impedance matching for robotic capture of a non-cooperative satellite. *Advanced Robotics*, 18(2):175–198, 2004.
14. E. Schmerling, L. Janson, and M. Pavone. Optimal sampling-based motion planning under differential constraints: the drift case with linear affine dynamics. In *Proc. IEEE Conf. on Decision and Control*, 2015.
15. Donald E Kirk. *Optimal control theory: an introduction*. Courier Corporation, 2012.